




## Article

# FeTiO<sub>3</sub> Perovskite Nanoparticles for Efficient Electrochemical Water Splitting

Periyannan Kaleeswarran <sup>1,†</sup>, Murugesan Praveen Kumar <sup>2,3,†</sup>, Ramalinga Viswanathan Mangalaraja <sup>4</sup>, Unalome Wetwatana Hartley <sup>3</sup>, Moorthy Sasikumar <sup>5</sup>, Rajasudha Venugopalan <sup>6</sup>, Manavalan Rajesh Kumar <sup>7</sup>, Jothi Ramalingam Rajabathar <sup>8</sup>, Shaik Gouse Peera <sup>9,\*</sup> and Govindhasamy Murugadoss <sup>10,\*</sup>

<sup>1</sup> Department of Nanoscience and Technology, Alagappa University, Karaikudi 630003, Tamilnadu, India; kaleeswarran@gmail.com

<sup>2</sup> CSIR-Central Electrochemical Research Institute (CSIR-CECRI), Karaikudi 630003, Tamilnadu, India; praveenkumarmurugesan280589@gmail.com

<sup>3</sup> Mechanical and Process Engineering Department, Sirindhorn International Institute of Technology, King Mongkut's University of Technology North Bangkok, Bangkok 10800, Thailand; unalome.w.cpe@tggs-bangkok.org

<sup>4</sup> Laboratory of Advanced Ceramics and Nanotechnology, Department of Materials Engineering, University of Concepción, Concepción 4030000, Chile; mangal@udec.cl

<sup>5</sup> Department of Physics, Bishop Heber College, Thiruchirappalli 620017, Tamilnadu, India; sasikumar.ph@bhc.edu.in

<sup>6</sup> Department of Chemistry, Bonsecours College for women, Thanjavur 613006, Tamilnadu, India; rajasudhathanjavur30@gmail.com

<sup>7</sup> Institute of Natural Science and Mathematics, Ural Federal University, 620002 Yekaterinburg, Russia; rajeshkumar\_vgm@yahoo.com

<sup>8</sup> Chemistry Department, College of Science, King Saud University, P.O. Box. 2455, Riyadh 11451, Saudi Arabia; jrajabathar@ksu.edu.sa

<sup>9</sup> Department of Environmental Science, Keimyung University, 1095 Dalgubeol-daero, Dalseo-gu, Daegu 42601, Korea

<sup>10</sup> Centre for Nanoscience and Nanotechnology, Sathyabama Institute of Science and Technology, Chennai 600119, Tamilnadu, India

\* Correspondence: gouse@kmu.ac.kr (S.G.P.); murugadoss\_g@yahoo.com (G.M.)

† Equally contributed author in this work.



**Citation:** Kaleeswarran, P.; Praveen Kumar, M.; Mangalaraja, R.V.; Hartley, U.W.; Sasikumar, M.; Venugopalan, R.; Rajesh Kumar, M.; Rajabathar, J.R.; Peera, S.G.; Murugadoss, G. FeTiO<sub>3</sub> Perovskite Nanoparticles for Efficient Electrochemical Water Splitting. *Catalysts* **2021**, *11*, 1028. <https://doi.org/10.3390/catal11091028>

Academic Editor: Weilin Dai

Received: 5 August 2021

Accepted: 24 August 2021

Published: 26 August 2021

**Publisher's Note:** MDPI stays neutral with regard to jurisdictional claims in published maps and institutional affiliations.



**Copyright:** © 2021 by the authors. Licensee MDPI, Basel, Switzerland. This article is an open access article distributed under the terms and conditions of the Creative Commons Attribution (CC BY) license (<https://creativecommons.org/licenses/by/4.0/>).

**Abstract:** The use of water splitting has been investigated as a good alternate for storing electrical energy. While the general interest in developing non-toxic, high-performance, and economically feasible catalysts for oxygen evolution reaction (OER) is noteworthy, there is also significant interest in water splitting research. Recently, perovskite-type oxides have performed as an alternative to non-precious metal catalysts and can act as a new class of effective catalysts in water splitting systems. Herein, a perovskite-structured FeTiO<sub>3</sub> was prepared via a facile one-step solvothermal method using ionic liquid as templates. The results of structural and morphological studies have supported the formation of FeTiO<sub>3</sub> perovskite. Furthermore, FeTiO<sub>3</sub> perovskite demonstrated OER activity with a lower onset potential of 1.45 V vs. RHE and Tafel slope value of 0.133 V.dec<sup>-1</sup> at 1 M KOH solution using mercury/mercurous oxide (Hg/HgO) were used as working electrodes.

**Keywords:** ionic liquids; solvothermal method; FeTiO<sub>3</sub>; hybrid electrocatalyst; OER; water splitting

## 1. Introduction

Hydrogen has long been considered as an alternative renewable energy carrier to replace fossil-fuel-based energy, with its zero-emission energy source. The electrocatalytic water splitting, which includes both an oxygen evolution reaction (OER) and a hydrogen evolution reaction (HER), is regarded as a significant opportunity for the zero-carbon hydrogen synthesis from the water [1]. CO<sub>2</sub> radioactive forcing from fossil fuel ignition exalted thermal discharge on large proportion due to its longer lifetime [2]. Considering

environmental protection and in order to safeguard the depletion of non-renewable energy resources, interest in clean alternative energies has been intensively focused. In recent years, the carbon-neutral energy system received impressive advancements in the field of renewable energy due to its clean repository. Attainment in the production of hydrogen is directly proportional to the efficiency of hydrogen produced and the use of hydrogen in energy conversion devices [3]. Comparably, electrochemical water electrolysis delivers an eco-friendly method to produce hydrogen as one of the energy transporters in the form of a chemical bond between two hydrogens and oxygen [4]. An alkaline condition of water splitting results in large quantities of pure hydrogen production, where it can be converted into storable combustible fuel in metal-air batteries and H<sub>2</sub>/O<sub>2</sub> fuel cells to produce energy [5,6].

The development of highly operative, noble metal-free and reliable OER catalyst is a challenging one. A potent electrocatalyst relies on an increase in the reaction rate and control of the electron transfer kinetic rate. So far, only a few potential catalysts such as Pt, IrO<sub>2</sub> and RuO<sub>2</sub> were identified as efficient functional materials for OER activity catalyst [7,8]. However, the inadequateness of noble metals and the high cost of the main blocks affect practical development. Thus, it is important to develop an alternate electrocatalyst with a lower cost, higher abundance and with greater efficiency [9]. Exceptional interest in nanostructured spinel oxides has been found to be a favorable electrode material for various electrochemical applications due to their superior electrochemical activity and chemical stability compared to the monometal oxide counterparts [10]. A transition metal ferrite, with a general formula of MFe<sub>2</sub>O<sub>4</sub> (M = Co, Ni, Cu, etc.), constitutes an important class of spinel oxides, due to the fascinating wide range of desirable surfaces, dimensions, and chemical compositions, which can produce versatile catalytic, electrical, optical, and mechanical properties for the electrocatalytic applications. The application of electrocatalysts is still faced with several limitations, among which the ferrites nanoparticles (NPs) tend to aggregate in the electrochemical redox process, which decreases the number of active sites for electrocatalysis and thereby causes an inadequate use of active materials. As a result, the overall performance of the electrocatalysts and their long-term structure stability is diminished [11].

Recently, perovskite-type oxides have obtained the significant consideration due to their solid crystal structure and have high electronic conductivity and catalytic activity. Perovskite materials are arranged in the matrix of crystalline structure with ABO<sub>3</sub>, where A is a large cation usually an alkali or alkaline earth metal and B is a small cation of transition metals [12]. Titanium dioxide (TiO<sub>2</sub>) has received great interest due to its superior chemical stability, nontoxicity, low cost and abundant nature. These properties also tend to produce conceivable material for photocatalytic degradation of organic dyes, solar cells, drug carriers, sodium-ion capacitors, sensors [13–17]. However, TiO<sub>2</sub> is inactive for OER due to lack of oxidation species, but it can be support for ilmenite type mixed oxides. The MTiO<sub>3</sub> nanomaterials can be synthesized via thermal treatment, solvothermal, chemical precipitation methods using various templates such as zeolites, ionic liquids. Obviously, ionic liquids (ILs) are preferred in the field of green chemistry due to their distinctive features such as recyclability, substantial temperature, considerable thermal stability and superior ionic conductivity. The recent advancement in ILs is desirable for the synthesis of nanomaterials with unique morphology via the solvothermal method [18]. Iron-based titanium oxides with formulating Z-scheme heterostructures of anodes have received great importance due to their strong electronic, magnetic and catalytic behaviors [19,20]. Moreover, the FeTiO<sub>3</sub> group of the crystalline structure is similar to corundum (Al<sub>2</sub>O<sub>3</sub>), which has trigonal symmetry and an R3 ilmenite crystal structure. This structure is distinguished by its ferroelectric properties, results from the degree of distortion experienced by octahedral clusters and the asymmetry between both the cations A and B along with the c axis. This will lead to a high active surface area of the material and superior electrochemical oxidation of water. In this present study, FeTiO<sub>3</sub> perovskite was formulated via a simple solvothermal reaction, the physical and chemical characteristics of the obtained samples

were tested using analytical techniques. Their electrocatalytic activity was also calculated towards OER in an alkaline media, the response of TiO<sub>2</sub> nanorod,  $\alpha$ -Fe<sub>2</sub>O<sub>3</sub> NPs and FeTiO<sub>3</sub> perovskite measured in order to attain ideal electrocatalytic activity.

## 2. Results and Discussion

Figure 1 illustrates the powder XRD patterns of TiO<sub>2</sub> nanorod,  $\alpha$ -Fe<sub>2</sub>O<sub>3</sub> NPs and FeTiO<sub>3</sub> perovskite. The planes of TiO<sub>2</sub> is clearly seen at a 2 $\theta$  of 35.3°, 38.6°, 40.3°, 53.0°, 63.2°, 70.2°, and 76.0° corresponding to (1 0 1)-TiO, (2 0 0)-Ti, (1 1 1)-TiO, (2 1 1)-Ti, (3 1 0)-Ti, (3 1 1)-Ti and (2 0 2)-TiO planes, respectively, as shown in Figure 1a [15]. Figure 1b shows the major XRD peaks presented at 24.1° (0 1 2), 33.1° (1 0 4), 35.5° (1 1 0), 40.7° (1 1 3), 49.2° (0 2 4), 53.8° (1 1 6), 57.4° (1 3 1), 62.2° (2 1 4) and 63.8° (3 0 0) of  $\alpha$ -Fe<sub>2</sub>O<sub>3</sub> NPs (JCPDS data Card No.: 00-001-1053). Furthermore, the XRD peaks of FeTiO<sub>3</sub> perovskite are obtained as displayed in Figure 1c. In the perovskite, the  $\alpha$ -Fe<sub>2</sub>O<sub>3</sub> NPs peak of 24.1° shifted toward 24.4° (0 0 2), and the intensity of 40.7° and 62.2° peaks were decreased due to composite of TiO<sub>2</sub> with  $\alpha$ -Fe<sub>2</sub>O<sub>3</sub> (JCPDS data Card No.: 00-047-0465) [21].

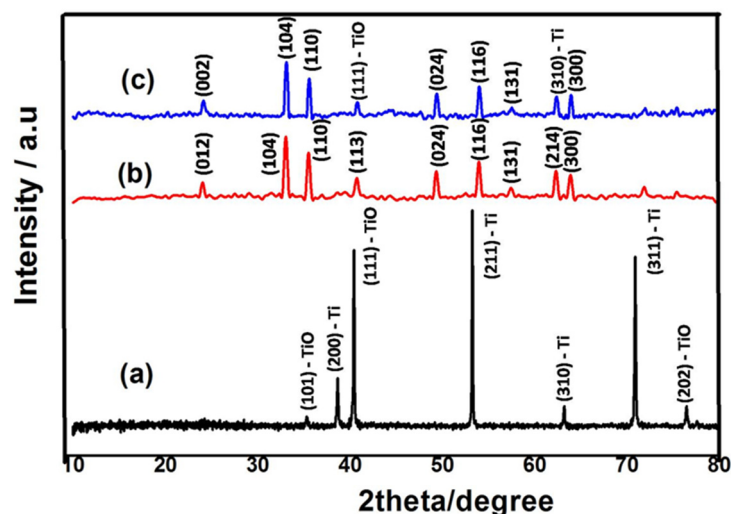
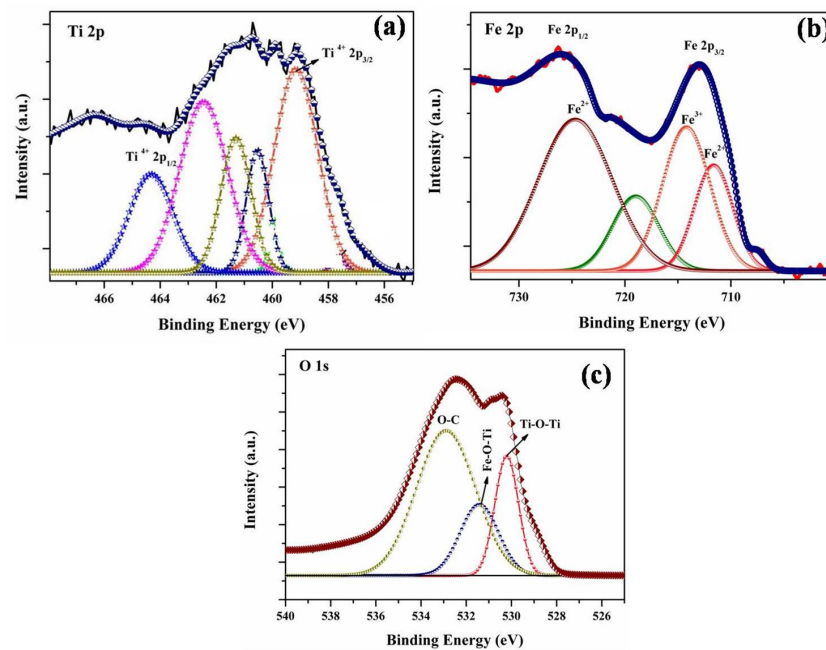


Figure 1. XRD patterns of TiO<sub>2</sub> nanorod (a),  $\alpha$ -Fe<sub>2</sub>O<sub>3</sub> NPs (b), and FeTiO<sub>3</sub> (c).

In order to investigate compositional and oxidation information, the XPS analysis was carried out for the FeTiO<sub>3</sub>. Here, Figure 2 represents the high-resolution spectra of Ti, Fe and O for FeTiO<sub>3</sub>. The doublet peaks at 458.6 eV (Ti 2p<sub>3/2</sub>) and 464.4 eV (Ti 2p<sub>1/2</sub>) as shown in Figure 2a [22]. The additional peaks of Ti 2p<sub>1/2</sub> at binding energies of 460.2, 461.3 and 462.4 eV are corresponding to Ti<sup>3+</sup> in FeTiO<sub>3</sub>. This designates the presence of TiO<sub>2</sub> in the film. The high-resolution spectrum of Fe is shown in Figure 2b. The peaks are appeared at 710 and 715 eV for Fe 2p<sub>3/2</sub> and Fe 2p<sub>1/2</sub>, respectively. The binding energy at 714.5 and 711.5 eV proceeded with the formation of Fe<sup>2+</sup>, and the peaks appeared at 715.2 eV for Fe<sup>3+</sup> in FeTiO<sub>3</sub> perovskite. Hence, the result confirmed the formation of Fe<sub>2</sub>O<sub>3</sub> in the perovskite. Figure 2c shows the high-resolution spectrum of O 1s. The deconvolution peaks are presented at 530.2, 531.5 and 533.5 eV correspond to Ti–O–Ti, Fe–O–Ti and O–C, which further confirmed the formation of FeTiO<sub>3</sub> perovskite.



**Figure 2.** Represents high resolution XPS spectra of (a) Ti2p, (b) Fe2p and (c) O1s of FeTiO<sub>3</sub> perovskite.

Figure 3 shows the surface morphology and microstructure analysis of the TiO<sub>2</sub> nanorod,  $\alpha$ -Fe<sub>2</sub>O<sub>3</sub> NPs and FeTiO<sub>3</sub> perovskite. Figure 3a reveals that TiO<sub>2</sub> is formed in the rod shape, Fe<sub>2</sub>O<sub>3</sub> is formed as microspheres structure (Figure 3b), and FeTiO<sub>3</sub> showed a mixed structure of rods and spherical particles (Figure 3c). The energy dispersive X-ray analysis (EDAX) spectra for TiO<sub>2</sub> nanorod,  $\alpha$ -Fe<sub>2</sub>O<sub>3</sub> NPs and FeTiO<sub>3</sub> show the presence of Ti, Fe and O Figure 3a<sub>1</sub>–c<sub>1</sub>. Figure 3a<sub>1</sub> confirmed the presence of Ti and O in TiO<sub>2</sub> nanorods. Further, the EDAX spectrum of  $\alpha$ -Fe<sub>2</sub>O<sub>3</sub> NPs showed the presence of Fe and O elements (Figure 3b<sub>1</sub>). Moreover, Fe, Ti and O elements are observed in the EDAX spectrum of FeTiO<sub>3</sub> (Figure 3c<sub>1</sub>), which confirmed the formation of NPs.

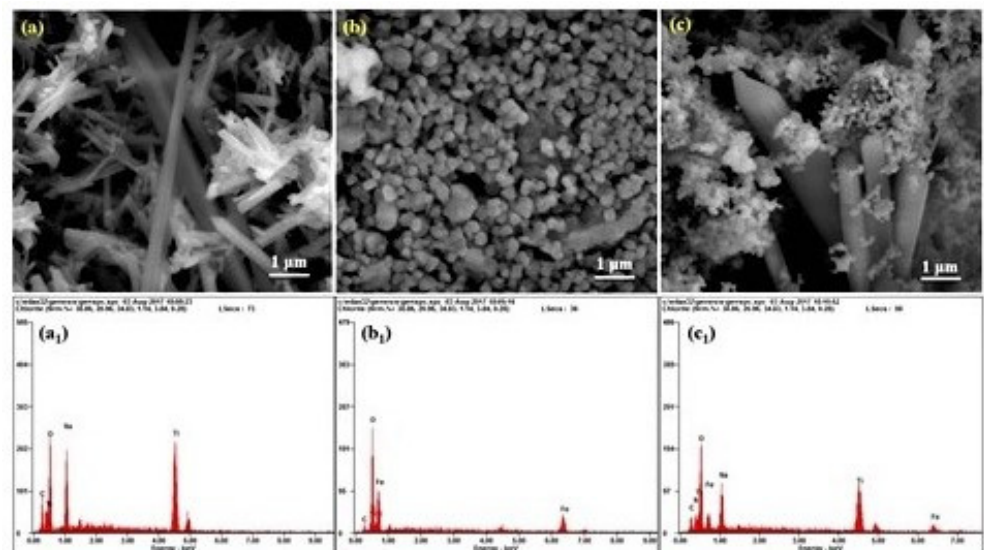


**Figure 3.** Shows FE-SEM images of (a) TiO<sub>2</sub> nanorod, (b)  $\alpha$ -Fe<sub>2</sub>O<sub>3</sub> NPs, (c) FeTiO<sub>3</sub> NPs, and (a<sub>1</sub>–c<sub>1</sub>) their corresponding EDAX spectrum.

The TEM image of TiO<sub>2</sub> nanorod is revealed in Figure 4a and the subsequently selected area electron diffraction (SAED) pattern is shown in Figure 4a<sub>1</sub>. The SAED pattern represents a highly crystalline TiO<sub>2</sub> nanorod with 10 nm thickness and few micrometers

in length. For  $\alpha$ -Fe<sub>2</sub>O<sub>3</sub> NPs, a fine surface with ~100 nm size as shown in Figure 4b and polycrystalline directly envisioned in the SAED pattern (Figure 4b<sub>1</sub>), while in FeTiO<sub>3</sub> a mixed structure of rod and spherical with aggregate morphology is observed as shown in Figure 4c. Furthermore, the SAED pattern confirmed the formation of polycrystalline (Figure 4c<sub>1</sub>).

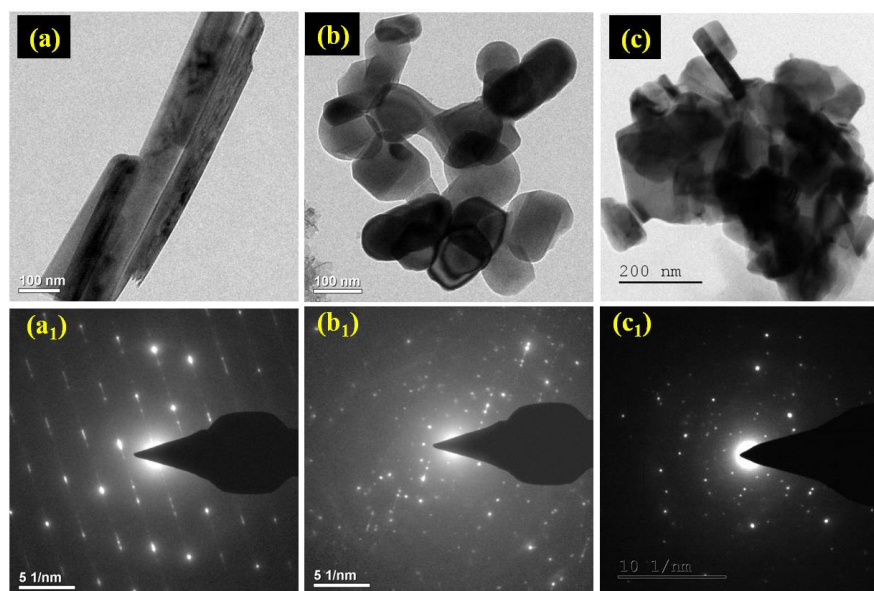


**Figure 4.** Shows TEM images of (a) TiO<sub>2</sub> nanorod, (b)  $\alpha$ -Fe<sub>2</sub>O<sub>3</sub> NPs, (c) FeTiO<sub>3</sub> perovskite, and (a<sub>1</sub>–c<sub>1</sub>) their corresponding SAED pattern.

The OER activities of TiO<sub>2</sub> nanorod,  $\alpha$ -Fe<sub>2</sub>O<sub>3</sub> NPs and FeTiO<sub>3</sub> perovskite were investigated using linear sweep voltammetry (LSV) in a three-electrode system as shown in Figure 5. The FeTiO<sub>3</sub> perovskite nanoparticles coated on Toray carbon sheet, platinum (Pt) rod, and mercury/mercurous oxide (Hg/HgO) were used as working, counter, and reference electrodes, respectively. In all the measurements, the potential of Hg/HgO was converted into reversible hydrogen electrode (RHE) using the formula [23],

$$E_{(\text{RHE})} = E^0_{(\text{Hg}/\text{HgO})} + E_{(\text{observed})} + 0.059\text{pH V} \quad (1)$$

$$\eta = E_{(\text{RHE})} - 1.23 \text{ V} \quad (2)$$

Noticeably, FeTiO<sub>3</sub> perovskite exhibits superior OER performance than TiO<sub>2</sub> nanorod and  $\alpha$ -Fe<sub>2</sub>O<sub>3</sub> NPs (Figure 5a). The FeTiO<sub>3</sub> shows the lowest onset potential of 1.45 V and the current density of 30 mA/cm<sup>2</sup> (Figure 5a). Furthermore, the overpotential ( $\eta$ ) of FeTiO<sub>3</sub> is 0.22 V, which is very low potential compared to  $\alpha$ -Fe<sub>2</sub>O<sub>3</sub> NPs (1.55 V), and TiO<sub>2</sub> nanorod is inactive. FeTiO<sub>3</sub> also displays less Tafel slope value of 0.133 V·dec<sup>-1</sup> compare to  $\alpha$ -Fe<sub>2</sub>O<sub>3</sub> NPs (0.240 V dec<sup>-1</sup>) (Figure 5b). Besides, TiO<sub>2</sub> nanorod and  $\alpha$ -Fe<sub>2</sub>O<sub>3</sub> NPs as supports have less activity as shown in Figure 5a. The onset potential of 1.55 V is gradually increased and no further activity is observed for  $\alpha$ -Fe<sub>2</sub>O<sub>3</sub> NPs and TiO<sub>2</sub> when using the single-channel electrocatalysts, as shown in Figure 5a,b. It is clear from this finding that the formation is inherently more efficient at improving the electron transport and improving the interaction between Fe and TiO<sub>2</sub> by the higher electronic conductivity of Ti and surface area [24]. The better performance of FeTiO<sub>3</sub> is due to Ti, which can be supported to avoid the further oxidation of Fe during the OER process. Figure 5c represents the comparison plot of onset potential, over potential and Tafel slope value for  $\alpha$ -Fe<sub>2</sub>O<sub>3</sub> NPs and FeTiO<sub>3</sub>. Moreover, the stability test was measured by the chronoamperometry technique at 1.5 V. FeTiO<sub>3</sub> shows high stability for 6 h which is comparable for IrO<sub>2</sub> as shown in Figure 5d [24,25]. After 6 h, the catalyst current was slightly declined due to the disturbance of catalyst surface

morphology. The evolution of O<sub>2</sub> was disturbed the interaction between nanoparticles and nanorods. Table 1 shows a comparison of OER activity for various catalysts in an alkaline medium.

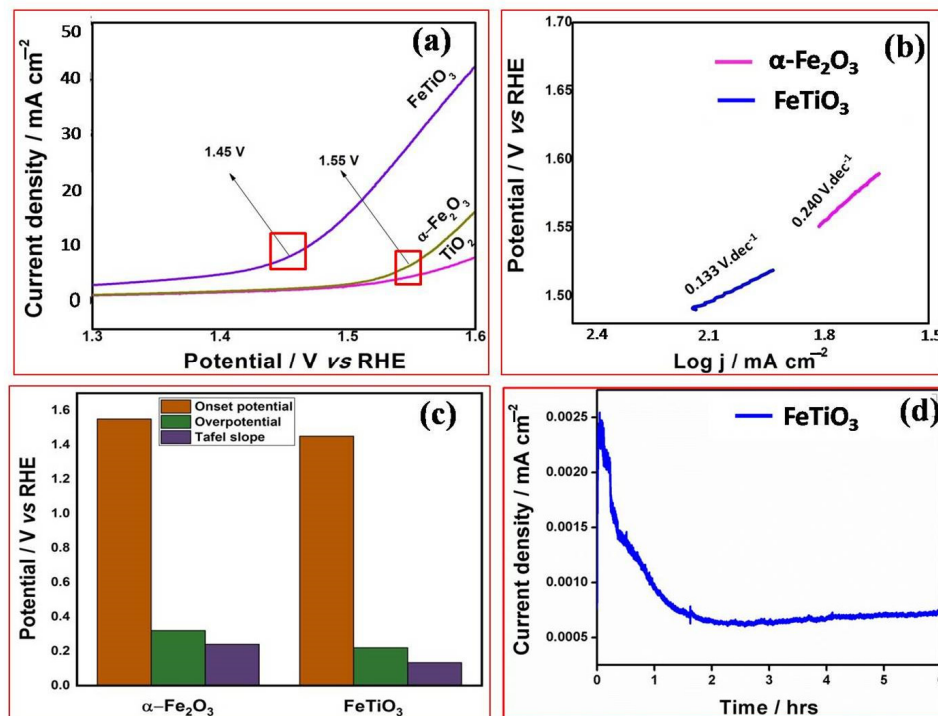


**Figure 5.** Shows (a) LSV of TiO<sub>2</sub> nanorod, α-Fe<sub>2</sub>O<sub>3</sub> NPs and FeTiO<sub>3</sub> perovskite, (b) Tafel slope values of α-Fe<sub>2</sub>O<sub>3</sub> NPs and FeTiO<sub>3</sub>, (c) comparison plot TiO<sub>2</sub>, α-Fe<sub>2</sub>O<sub>3</sub> and FeTiO<sub>3</sub> perovskite and (d) chronoamperometry study FeTiO<sub>3</sub> perovskite.

**Table 1.** Comparison of onset potential of various catalysts for OER.

S. No.	Catalyst	Medium	Onset Potential (V vs. RHE)	Reference
1.	g-C <sub>3</sub> N <sub>4</sub> @Ni-NiO	0.1 M NaOH	1.55	[23]
2.	FeTiO <sub>3</sub> hollow spheres	1 M KOH	1.65	[26]
3.	CoTiO <sub>3</sub> /NrGO	0.1 M NaOH	1.53	[27]
4.	B-doped graphene	0.1 M NaOH	1.70	[28]
5.	FeTiO <sub>3</sub>	1 M KOH	1.45	This work

### 3. Materials and Methods

#### 3.1. Materials

Ferric chloride hexahydrate (FeCl<sub>3</sub>·6H<sub>2</sub>O), ferrous sulfate (FeSO<sub>4</sub>·7H<sub>2</sub>O), titanium (IV) isopropoxide Ti(OCH(CH<sub>3</sub>)<sub>2</sub>)<sub>4</sub> (TIP) were supplied by Sigma-Aldrich Bengaluru, Karnataka 560099, India, 1-butyl-3-methylimidazolium bromide (C<sub>8</sub>H<sub>15</sub>BrN<sub>2</sub>) (IL) was purchased from TCI Chemicals (Chennai, Tamil Nadu 600045, India) and, ethylene glycol (HOCH<sub>2</sub>CH<sub>2</sub>OH) (EG) and sodium hydroxide (NaOH) were obtained from Merck (Mumbai- 400079, India). All of the chemicals used were of the highest analytical quality, and no further purification was required.

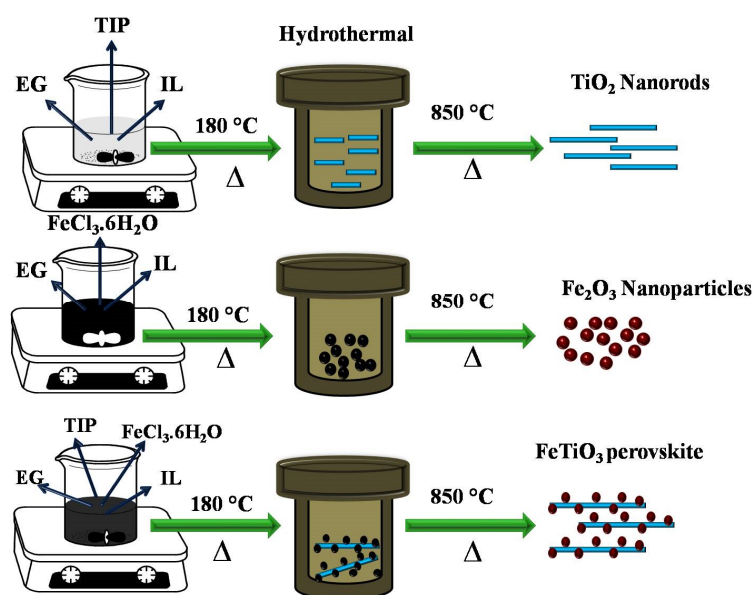
#### 3.2. Preparation of TiO<sub>2</sub> Nanorod

The pure TiO<sub>2</sub> was synthesized by an effortless solvothermal process. In brief, 0.1 M of Ti (OCH(CH<sub>3</sub>)<sub>2</sub>)<sub>4</sub> as a source of TiO<sub>2</sub> was first dissolved in 50 mL of ethylene glycol and

0.015 M of  $C_8H_{15}BrN_2$  was mixed with the above solution under continuous stirring for 2 h. Then, 1.0 M/L NaOH solution was added dropwise to adjust pH to 12.0. The solution was transferred into 100 mL volume of a Teflon-lined stainless-steel autoclave and then it was heated at 180 °C for 24 h. Subsequently cool down to room temperature, then the resultant suspensions were washed several times with water and ethanol to remove the unreacted species, and then the final product was dried at 100 °C for 2 h. Finally,  $TiO_2$  nanorods were obtained by calcined in air at 850 °C for 5 h.

### 3.3. Synthesis of $FeTiO_3$ Perovskite

$\alpha$ - $Fe_2O_3$  NPs and  $FeTiO_3$  perovskite were prepared by facile solvothermal method. The detailed process is explained as follows: 0.050 M of  $FeCl_3 \cdot 6H_2O$  and 0.050 M of  $FeSO_4 \cdot 7H_2O$  ( $\alpha$ - $Fe_2O_3$  sources) were dissolved in ethylene glycol under magnetic stirring for 30 min at room temperature, additionally 0.1 M of  $Ti(OCH(CH_3)_2)_4$  was further added to form the homogenous solution. Thereafter, 0.015 M of  $C_8H_{15}BrN_2$  was added to the above mixture under vigorous stirring. The pH value was adjusted to 12 by using NaOH. Subsequently, the mixture was transferred into a Teflon-lined stainless-steel autoclave and heated in an electric oven at 180 °C for 24 h. The resultant suspensions were washed several times with water and ethanol to remove the unreacted species in the final product and then dried at 60 °C for 12 h. Finally,  $FeTiO_3$  perovskite was obtained by calcination in air at 850 °C for 5 h as shown in Scheme 1. The same producer was used for the synthesis of  $\alpha$ - $Fe_2O_3$  NPs without adding titanium sources.



**Scheme 1.** Schematic representation of  $TiO_2$  nanorod,  $\alpha$ - $Fe_2O_3$  NPs and  $FeTiO_3$  synthesis via a one-step solvothermal method.

### 3.4. Electrochemical Studies

The electrochemical studies were investigated using a Bio-Logic instrument (Seyssinet-Pariset, France) with the three electrode systems for OER in 1 M KOH. Linear sweep voltammogram (LSV) was observed at 10  $mV s^{-1}$  to reduce the capacitive current, which is directly proportional to the scan rate. The stability test was measured by the chronoamperometry technique at 1.5 V.  $FeTiO_3$  perovskite nanoparticles coated on a Toray carbon sheet, platinum (Pt) rod, and mercury/mercurous oxide (Hg/HgO) were used as working, counter, and reference electrodes, respectively.

### 3.5. Characterization

The X-ray diffraction (XRD) was measured for all the samples using  $Cu-K\alpha$  radiation with the wavelength of 1.54060 Å by PAN analytical (Malvern Analytical, Malvern, Eng-

land) (XPRT-PRO) diffractometer in the 2 theta range from 10° to 80°. The morphology of prepared samples was recorded using field emission scanning electron microscopy (FE-SEM: Model Hitachi S-4500, Carl Zeiss NTS Ltd. Jena, Germany) equipped with the energy-dispersive X-ray spectroscopy (EDAX). The transmission electron microscopy (TEM) and selected area electron diffraction (SAED) were carried out to investigate the morphology and crystalline nature of the samples (Tecnai Instruments). The X-ray photoelectron spectroscopy (XPS) was carried out using the XPS instrument (Carl Zeiss). The spectra were at pressure using an ultra-high vacuum with Al K $\alpha$  excitation wavelength at 250 W. The electrochemical studies were investigated by using a Bio-Logic instrument with the three electrode systems for OER in 1 M KOH.

#### 4. Conclusions

FeTiO<sub>3</sub> perovskite was developed using a one-step solvothermal method. The proposed method facilitated in reducing the onset potential and increased the current density for OER in an alkaline solution. The formation of FeTiO<sub>3</sub> was confirmed using XRD, XPS and TEM studies. FeTiO<sub>3</sub> demonstrated a high OER activity compared to the bare TiO<sub>2</sub> nanorod and  $\alpha$ -Fe<sub>2</sub>O<sub>3</sub> NPs. The onset potential of FeTiO<sub>3</sub> was 1.45 V with a current density of 30 mA/cm<sup>2</sup>, which were comparable to the benchmark catalyst of IrO<sub>2</sub>. Furthermore, the catalyst was highly stable for 6 h in 1M KOH solution. Therefore, the prepared FeTiO<sub>3</sub> perovskite could be considered as an effective catalyst for water electrolyzer technology in the future.

**Author Contributions:** P.K. and M.P.K. contributed to methodology, investigation, writing—original draft preparation; R.V.M. contributed to validation, data curation, formal analysis; U.W.H. contributed to data curation, formal analysis; M.S. contributed to software, data curation; R.V. and M.R.K. contributed to formal analysis, data curation; J.R.R. contributed to formal analysis; S.G.P. contributed to formal analysis, validation; G.M. conceptualized the overall idea of this research, supervision, writing—review and editing, visualization, data curation. Finally, G.M. reviewed, edited and submitted the manuscript in the final form. All authors have read and agreed to the published version of the manuscript.

**Funding:** This research received no external funding.

**Data Availability Statement:** Data available on request from the authors.

**Acknowledgments:** The author G.M. thanks the Chancellor, President, and Vice Chancellor, Sathyabama Institute of Science and Technology, Chennai for the support and encouragement. The author J.R.R. thanks the Researchers Supporting Project Number (RSP-2021/354), King Saud University, Riyadh, Saudi Arabia for the financial support. The author S.G.Peera also thank research support from the National Research Foundation of Korea (NRF) funded by the Korean government, Ministry of Science and ICT (MSIT) (No. 2021R1F1A1046648), Republic of Korea.

**Conflicts of Interest:** The authors declare no conflict of interest.

#### References

1. Wu, A.; Xie, Y.; Ma, H.; Tian, C.; Gu, Y.; Yan, H.; Zhang, X.; Yang, G.; Fu, H. Integrating the active OER and HER components as the heterostructures for the efficient overall water splitting. *Nano Energy* **2018**, *44*, 353–363. [[CrossRef](#)]
2. Zhang, X.; Caldeira, K. Time scales and ratios of climate forcing due to thermal versus carbon dioxide emissions from fossil fuels. *Geophys. Res. Lett.* **2015**, *42*, 4548–4555. [[CrossRef](#)]
3. Stamenkovic, V.R.; Strmcnik, D.; Lopes, P.P.; Markovic, N.M. Energy and fuels from electrochemical interfaces. *Nat. Mater.* **2017**, *16*, 57–69. [[CrossRef](#)] [[PubMed](#)]
4. Gholipour, M.R.; Dinh, C.T.; B eland, F.; Do, T.O. Nanocomposite heterostructures as sunlight-driven photocatalysts for hydrogen production from water splitting. *Nanoscale* **2015**, *7*, 8187–8208. [[CrossRef](#)] [[PubMed](#)]
5. Zhan, Y.; Lu, M.; Yang, S.; Liu, Z.; Lee, J.Y. The origin of catalytic activity of nickel phosphate for oxygen evolution in alkaline solution and its further enhancement by iron substitution. *ChemElectroChem* **2016**, *3*, 615–621. [[CrossRef](#)]
6. Zaffora, A.; Santamaria, M.; Di Franco, F.; Habazaki, H.; Di Quarto, F. Photoelectrochemical evidence of inhomogeneous composition at nm length scale of anodic films on valve metals alloys. *Electrochim. Acta.* **2016**, *201*, 333–339. [[CrossRef](#)]
7. Koza, J.A.; He, Z.; Miller, A.S.; Switze, J.A. Electrodeposition of crystalline Co<sub>3</sub>O<sub>4</sub>-A Catalyst for the Oxygen Evolution Reaction. *Chem. Mater.* **2012**, *24*, 3567–3573. [[CrossRef](#)]



8. Tian, J.; Liu, Q.; Asiri, A.M.; Sun, X. Self-supported nanoporous cobalt phosphide nanowire arrays: An efficient 3D hydrogen-evolving cathode over the wide range of pH 0–14. *J. Am. Chem. Soc.* **2014**, *136*, 7587–7590. [[CrossRef](#)]
9. Dutta, A.; Pradhan, N. Developments of metal phosphides as efficient OER precatalysts. *J. Phys. Chem. Lett.* **2017**, *8*, 144–152. [[CrossRef](#)]
10. Kaleeswarran, P.; Sriram, B.; Wang, S.F.; Baby, J.N.; Arumugam, A.; Bilgrami, A.L.; Hashsham, S.A.; Sayegh, F.A.; Liu, C.J. Electrochemical detection of antipsychotic drug in water samples based on nano/sub-microrod-like  $\text{CuBi}_{2-x}\text{In}_x\text{O}_4$  electrocatalysts. *Microchem. J.* **2021**, *163*, 105886. [[CrossRef](#)]
11. Li, M.; Xiong, Y.; Liu, X.; Bo, X.; Zhang, Y.; Han, C.; Guo, L. Facile synthesis of electrospun  $\text{MFe}_2\text{O}_4$  (M = Co, Ni, Cu, Mn) spinel nanofibers with excellent electrocatalytic properties for oxygen evolution and hydrogen peroxide reduction. *Nanoscale* **2015**, *7*, 8920–8930. [[CrossRef](#)]
12. Suntivich, J.; Gasteiger, H.A.; Yabuuchi, N.; Nakanishi, H.; Goodenough, J.B.; Horn, Y.S. Design principles for oxygen-reduction activity on perovskite oxide catalysts for fuel cells and metal–air batteries. *Nat. Chem.* **2011**, *3*, 546–550. [[CrossRef](#)]
13. Murugadoss, G.; Jayavel, R.; Kumar, M.R. Systematic investigation of structural and morphological studies on doped  $\text{TiO}_2$  nanoparticles for solar cell applications. *Superlattices Microstruct.* **2014**, *76*, 349–361. [[CrossRef](#)]
14. Murugadoss, G.; Thangamuthu, R.; Vijayaraghavan, S.; Kanda, H.; Ito, S. Caesium-Methyl Ammonium Mixed-Cation Lead Iodide Perovskite Crystals: Analysis and Application for Perovskite Solar Cells. *Electrochim. Acta* **2017**, *257*, 267–280. [[CrossRef](#)]
15. Murugadoss, G.; Kanda, H.; Tanaka, S.; Nishino, H.; Ito, S.; Imahoric, H.; Umeyama, T. An efficient electron transport material of tin oxide for planar structure perovskite solar cells. *J. Power Sources* **2016**, *307*, 891–897. [[CrossRef](#)]
16. Manibalan, G.; Govindaraj, Y.; Yesuraj, J.; Kuppusami, P.; Murugadoss, G.; Murugavel, R.; Kumar, M.R. Facile synthesis of  $\text{NiO@Ni(OH)}_2\text{-}\alpha\text{-MoO}_3$  nanocomposite for enhanced solid-state symmetric supercapacitor application. *J. Colloid Interface Sci.* **2021**, *585*, 505–518. [[CrossRef](#)]
17. Manibalan, G.; Murugadoss, G.; Thangamuthu, R.; Kumar, R.M.; Jayavel, R. Facile synthesis of heterostructure  $\text{CeO}_2\text{-TiO}_2$  nanocomposites for enhanced electrochemical sensor and solar cell applications. *J. Alloy. Compd.* **2019**, *773*, 449–461. [[CrossRef](#)]
18. Zwara, J.; Paszkiewicz-Gawron, M.; Łuczak, J.; Pancielejko, A.; Lisowski, W.; Trykowski, G.; Zaleska-Medynska, A.; Grabowski, E. The effect of imidazolium ionic liquid on the morphology of Pt nanoparticles deposited on the surface of  $\text{SrTiO}_3$  and photoactivity of Pt- $\text{SrTiO}_3$  composite in the  $\text{H}_2$  generation reaction. *Int. J. Hydrogen Energy* **2019**, *44*, 26308–26321. [[CrossRef](#)]
19. Guo, S.; Wang, Y.; Chen, L.; Pan, D.; Guo, Z.; Xia, S. Porous  $\text{TiO}_2\text{-FeTiO}_3\text{@Carbon}$  nanocomposites as anode for high-performance lithium-ion batteries. *J. Alloys Compd.* **2021**, *858*, 157635. [[CrossRef](#)]
20. Aparna, T.K.; Sivasubramanian, R.  $\text{FeTiO}_3$  nano-hexagons based electrochemical sensor for the detection of dopamine in presence of uric acid. *Mater. Chem. Phys.* **2019**, *233*, 319–328. [[CrossRef](#)]
21. Gou, H.P.; Zhang, G.H.; Chou, K.C. Influence of Pre-oxidation on Carbothermic Reduction Process of Ilmenite Concentrate. *ISIJ Int.* **2015**, *55*, 928–933. [[CrossRef](#)]
22. Praveen Kumar, M.; Jagannathan, R.; Ravichandran, S. Photoelectrochemical system for unassisted high-efficiency water-splitting reactions using N-doped  $\text{TiO}_2$  Nanotubes. *Energy Fuels* **2020**, *34*, 9030–9036. [[CrossRef](#)]
23. Praveen Kumar, M.; Murugesan, P.; Vivek, S.; Ravichandran, S.  $\text{NiWO}_3$  Nanoparticles Grown on Graphitic Carbon Nitride ( $\text{g-C}_3\text{N}_4$ ) Supported Toray Carbon as an Efficient Bifunctional Electrocatalyst for Oxygen and Hydrogen Evolution Reactions. *Part. Part. Syst. Charact.* **2017**, *34*, 1700043–1700052. [[CrossRef](#)]
24. Badreldin, A.; Abusrafa, A.E.; Abdel-Wahab, A. Oxygen-deficient perovskites for oxygen evolution reaction in alkaline media: A review. *Emergent Mater.* **2020**, *3*, 567–590. [[CrossRef](#)]
25. Lu, X.; Zhao, C. Electrodeposition of hierarchically structured three-dimensional nickel–iron electrodes for efficient oxygen evolution at high current densities. *Nat. Commun.* **2015**, *6*, 1–7.
26. Han, T.; Chen, Y.; Tian, G.; Wang, J.Q.; Ren, Z.; Zhou, W.; Fu, H. Hierarchical  $\text{FeTiO}_3\text{-TiO}_2$  hollow spheres for efficient simulated sunlight-driven water oxidation. *Nanoscale* **2015**, *7*, 15924–15934. [[CrossRef](#)] [[PubMed](#)]
27. Luque-Centeno, J.M.; Martínez-Huerta, M.V.; Sebastián, D.; Pardo, J.I.; Lázaro, M.J.  $\text{CoTiO}_3\text{/NrGO}$  nanocomposites for oxygen evolution and oxygen reduction reactions: Synthesis and electrocatalytic performance. *Electrochim. Acta* **2020**, *331*, 135396. [[CrossRef](#)]
28. Vineesh, T.V.; Praveen Kumar, M.; Takahashi, C.; Kalita, G.; Alwarappan, S.; Pattanayak, D.K.; Narayanan, T.N. Bifunctional Electrocatalytic Activity of Boron-Doped Graphene Derived from Boron Carbide. *Adv. Energy Mater.* **2015**, *5*, 1500658–1500665. [[CrossRef](#)]